activity (Fig. 3B). Mutation of Phe155 to alanine severely impaired crRNA processing, suggesting that this residue also plays an important role in substrate orientation. However, none of the above mutations severely disrupted crRNA binding, as judged by means of electrophoretic mobility shift assays, indicating that the structural integrity of the mutant proteins was not compromised (fig. S8). Thus, interaction between Csy4 and the closing base pair of the RNA stem is critical for pre-crRNA processing, whereas sequence-specific recognition of the penultimate base pair in the stem is less important. Incubation of Csy4 with a panel of short RNA oligonucleotides containing a variety of mutations in the CRISPR repeat stem-loop sequence further confirmed that Csy4 requires a C-G base pair closing the RNA stem and that Csy4 can accommodate different nucleotides at the penultimate RNA base pair (fig. S10).

Phylogenetic analysis of CRISPR loci suggests that CRISPR repeat sequences and structures have co-evolved with the Cas genes (*19*). The similarity of Csy4 at the fold level to the CRISPR-processing endonucleases CasE and Cas6 suggests that collectively they are likely to have descended from a single ancestral endoribonuclease enzyme that has diverged throughout evolution. The structure described here reveals how Csy4 and related endonucleases from the same CRISPR/Cas subfamily use an exquisite recognition mechanism to discriminate crRNA substrates from other cellular RNAs. This illustrates the importance of co-evolution in shaping molecular recognition mechanisms in the CRISPR pathway. Furthermore, the ability of Csy4 to form a tight complex with the cleaved crRNA product points to Csy4 having a functional role within the CRISPR pathway that extends beyond pre-crRNA cleavage.

References and Notes

1. S. J. Brouns *et al.*, *Science* **321**, 960 (2008).
2. J. Carte, R. Wang, H. Li, R. M. Terns, M. P. Terns, *Genes Dev.* **22**, 3489 (2008).
3. D. H. Haft, J. Selengut, E. F. Mongodin, K. E. Nelson, *PLOS Comput. Biol.* **1**, e60 (2005).
4. C. R. Hale *et al.*, *Cell* **139**, 945 (2009).
5. K. S. Makarova, N. V. Grishin, S. A. Shabalina, Y. I. Wolf, E. V. Koonin, *Biol. Direct* **1**, 7 (2001).
6. R. Barrangou *et al.*, *Science* **315**, 1709 (2007).
7. L. A. Marraffini, E. J. Sontheimer, *Science* **322**, 1843 (2008).
8. L. A. Marraffini, E. J. Sontheimer, *Nat. Rev. Genet.* **11**, 181 (2010).
9. J. van der Oost, M. M. Jore, E. R. Westra, M. Lundgren, S. J. Brouns, *Trends Biochem. Sci.* **38**, 401 (2009).
10. R. Jansen, J. D. Embden, W. Gaastra, L. M. Schouls, *Mol. Microbiol.* **43**, 1565 (2002).
11. I. Grissa, G. Vergnaud, C. Pourcel, *BMC Bioinformat.* **8**, 172 (2007).
12. T. H. Tang *et al.*, *Proc. Natl. Acad. Sci. U.S.A.* **99**, 7536 (2002).
13. R. K. Lillestøl, P. Redder, R. A. Garrett, K. Brügger, *Archaea* **2**, 59 (2006).
14. R. K. Lillestøl *et al.*, *Mol. Microbiol.* **72**, 259 (2009).
15. T. H. Tang *et al.*, *Mol. Microbiol.* **55**, 469 (2005).
16. Materials and methods are available as supporting material on *Science* Online.
17. A. Ebihara *et al.*, *Protein Sci.* **15**, 1494 (2006).
18. L. Holm, C. Sander, *J. Mol. Biol.* **233**, 123 (1993).
19. V. Kunin, R. Sorek, P. Hugenholtz, *Genome Biol.* **8**, R61 (2007).
20. P. Legault, J. Li, J. Mogridge, L. E. Kay, J. Greenblatt, *Cell* **93**, 289 (1998).
21. A. Huppler, L. J. Nikstad, A. M. Allmann, D. A. Brow, S. E. Butcher, *Nat. Struct. Biol.* **9**, 431 (2002).
22. Z. Cai *et al.*, *Nat. Struct. Biol.* **5**, 203 (1998).
23. X. Ye, A. Gorin, A. D. Ellington, D. J. Patel, *Nat. Struct. Biol.* **3**, 1026 (1996).
24. K. Anand, A. Schulte, K. Vogel-Bachmayr, K. Scheffzek, M. Geyer, *Nat. Struct. Mol. Biol.* **15**, 1287 (2008).

25. We thank W. Westphal for help with purification of Csy4 constructs; J. van der Oost for discussion; J. Doudna Cate and members of the Doudna laboratory for critical reading of the manuscript; and C. Ralston and J. Holton (Beamlines 8.2.2 and 8.3.1, Advanced Light Source, Lawrence Berkeley National Laboratory) and S. Coyle for assistance with X-ray data collection. R.E.H. is supported by the U.S. NIH training grant 5 T32 GM08295. M.J. is supported by a Human Frontier Science Program Long-Term Fellowship. B.W. is a Howard Hughes Medical Institute Fellow of the Life Sciences Research Foundation. This work was supported in part by grants from NSF and the Bill and Melinda Gates Foundation. J.A.D. is a Howard Hughes Medical Institute Investigator. Coordinates and structure factors for the Csy4-crRNA complex have been deposited in the Protein Data Bank under accession codes 2xli, 2xlj, and 2xlk. The authors have filed a related patent.

Supporting Online Material

www.sciencemag.org/cgi/content/full/329/5997/1355/DC1
Materials and Methods
Figs. S1 to S10
Table S1
References

13 May 2010; accepted 22 July 2010
10.1126/science.1192272

Prediction of Individual Brain Maturity Using fMRI

Nico U. F. Dosenbach,[1]* Binyam Nardos,[1] Alexander L. Cohen,[1] Damien A. Fair,[2] Jonathan D. Power,[1] Jessica A. Church,[1] Steven M. Nelson,[1,3] Gagan S. Wig,[1,4,5] Alecia C. Vogel,[1] Christina N. Lessov-Schlaggar,[6] Kelly Anne Barnes,[1] Joseph W. Dubis,[1] Eric Feczko,[6] Rebecca S. Coalson,[1,7] John R. Pruett Jr.,[6] Deanna M. Barch,[3,6,7] Steven E. Petersen,[1,3,7,8] Bradley L. Schlaggar[1,7,8,9]*

Group functional connectivity magnetic resonance imaging (fcMRI) studies have documented reliable changes in human functional brain maturity over development. Here we show that support vector machine-based multivariate pattern analysis extracts sufficient information from fcMRI data to make accurate predictions about individuals' brain maturity across development. The use of only 5 minutes of resting-state fcMRI data from 238 scans of typically developing volunteers (ages 7 to 30 years) allowed prediction of individual brain maturity as a functional connectivity maturation index. The resultant functional maturation curve accounted for 55% of the sample variance and followed a nonlinear asymptotic growth curve shape. The greatest relative contribution to predicting individual brain maturity was made by the weakening of short-range functional connections between the adult brain's major functional networks.

Functional magnetic resonance imaging (fMRI) holds the promise that it may one day aid in the diagnosis of developmental delays and neuropsychiatric disorders, especially for conditions that lack structural brain abnormalities. Much progress has been made describing typical and atypical human brain activity at the group level with use of fMRI. However, determining whether single fMRI scans contain sufficient information to classify and make predictions about individuals remains a critical challenge (*1*).

The work described here had two major objectives. The first aim was to develop an approach for making accurate predictions about individuals on the basis of single fMRI scans. The second aim, building on the first, was to further illuminate typical brain development, a prerequisite for studying developmental disorders and pediatric-onset neuropsychiatric diseases (*2*, *3*).

Previous developmental fMRI studies have shown reliable differences between children and adults (*4*–*9*). Thus, we set out to push the study of functional brain maturation toward making predictions about single individuals. We used multivariate pattern analysis (MVPA) tools (*10*–*14*) to make continuously valued predictions about the relative functional maturity levels of individual brains.

[1]Department of Neurology, Washington University School of Medicine, St. Louis, MO 63110, USA. [2]Department of Psychiatry, Oregon Health and Science University, Portland, OR 97239, USA. [3]Department of Psychology, Washington University, St. Louis, MO 63130, USA. [4]Department of Psychology, Harvard University, Cambridge, MA 02138, USA. [5]Athinoula A. Martinos Center for Biomedical Imaging, Massachusetts General Hospital, Charlestown, MA 02129, USA. [6]Department of Psychiatry, Washington University School of Medicine, St. Louis, MO 63110, USA. [7]Department of Radiology, Washington University School of Medicine, St. Louis, MO 63110, USA. [8]Department of Anatomy and Neurobiology, Washington University School of Medicine, St. Louis, MO 63110, USA. [9]Department of Pediatrics, Washington University School of Medicine, St. Louis, MO 63110, USA.

*To whom correspondence should be addressed. E-mail: ndosenbach@wustl.edu (N.U.F.D.); schlaggarb@neuro.wustl.edu (B.L.S.)

MVPA applies sophisticated machine-learning algorithms (*12*, *14*) to the complex patterns generated by a myriad of measurements, termed features. We chose support vector machines (SVMs) as our classification and prediction algorithms because they are resilient to overfitting and allow the extraction of feature weights (*15*, *16*). Because of its sensitivity, MVPA has become increasingly used in task-evoked neuroimaging, beginning with early work by Haxby and colleagues (*10*). When applied to task-related fMRI data, MVPA has allowed researchers to accomplish impressive feats, such as extracting patterns related to memory reinstatement (*17*), predicting which nouns participants heard (*18*), and exploring the neural correlates of consciousness (*19*, *20*).

However, in many pediatric and clinical populations, the acquisition of task-related data becomes increasingly difficult because of a variety of causes (e.g., ability to perform task). Therefore, we used functional connectivity MRI (fcMRI) data, which can be collected quickly and easily under different conditions, including but not limited to anesthesia, sleep, and quiet rest (*21*). Resting-state fcMRI (rs-fcMRI) studies measure the correlations in spontaneous activity between brain regions (*22*). These rs-fcMRI measurements are reliable across scans and institutions (*23*) and are thought to have been shaped by the cumulative effect of experiences across one's lifespan (*24*).

Thus, we developed a functional connectivity MVPA (fcMVPA) approach that combines the sensitivity of MVPA with the robust and easy data acquisition of fcMRI. To build a machine that could predict the functional maturity level of individual brains from about 5 min of fMRI data, we used 238 rs-fcMRI scans (3 T; continuous rest) from typically developing participants ranging in age from 7 to 30 years (tables S1 and S2). Blood oxygen level–dependent (BOLD) time courses were generated for 160 regions of interest (ROIs) derived from a series of meta-analyses of task-related fMRI studies that cover much of the brain (fig. S1 and table S3). All possible interregional temporal correlations, or functional connections (n = 12,720), were computed for each individual. By using standard MVPA methodology to avoid circularity bias (*14*), we first reduced the number of features to the 200 functional connections most reliably different between children and adults in each round of leave-one-out cross-validation (*16*).

Binary SVM classification of individuals as either children (61 scans of 7- to 11-year-olds; mean = 9.4) or adults (61 scans of 24- to 30-year-olds; mean = 26.2), matched for brain volume and in-scanner movement, was 91% accurate (permutation test, $P < 0.0001$; 90% sensitive; 92% specific).

To assess the relative functional brain maturity of individuals more precisely, we used SVM regression (SVR). Chronological age served as the training measure for SVR brain maturity prediction because, in contrast to other potential measures of maturity such as hormone levels or developmental milestones, age is easily obtained and free of measurement error. In this manner, we generated a predicted "brain age" as an estimate of each participants' functional maturity level. Achieving functional brain maturity in this sense is likely the consequence of integrated processes that are both developmental (e.g., myelination and synaptic pruning) and experiential.

The predicted brain ages for all scans were converted to a functional connectivity maturation index (fcMI) by setting the mean predicted brain age of typically developed young adults (18 to 30 years old) equal to 1.0. The fcMI thus represents a 200-dimensional, weighted index of an individual's overall functional brain maturity.

Model selection analyses were carried out by using Akaike information criterion (AIC) weights (*16*, *25*). These analyses showed that functional maturity levels between the ages of 7 and 30 years, as measured by fcMI, are best fit by classic biological models of asymptotic growth or maturation (*26*), such as Von Bertalanffy's growth curve or the Pearl-Reed logistic growth curve (Fig. 1 and table S4).

The most probable models of functional brain maturation provided almost identical curve fits in the 7- to 30-years-old age range (Fig. 1 and fig. S2). Linear models generated the poorest fits (fig. S2 and table S4). The best fitting models showed asymptotic maturation toward a predicted population mean maximum brain age of ~22 years, corresponding to an fcMI of slightly greater than 1.0. The fitted models mainly differed in their predictions for younger ages. The two-parameter Von Bertalanffy curve predicts more rapid maturation between birth and age 7 years than the three-parameter Pearl-Reed curve. Future collection of additional rs-fcMRI scans between birth and age 7 years should help decide between these interesting alternatives.

For independent replication, the same analyses were also carried out on two other large-scale developmental functional connectivity data sets with somewhat different characteristics. Data set 2 consisted of 195 fcMRI scans (age 7 to 31 years; 1.5 T) where rest periods had been extracted from blocked fMRI designs. Data set 3 consisted of 186 event-related fMRI scans (age 6 to 35 years) that were made more similar to resting state by regressing out task effects. Despite these differences in the type of functional connectivity data, binary adult-versus-child classification results replicated (accuracy of 92% for data set 2 and 93% data set 3), as did the functional brain maturity prediction results (data set 2, $r^2 = 0.519$; data set 3, $r^2 = 0.557$) (figs. S3 and S4, and table S4). After separately generating fcMI values for each data set, 613 scans between the ages of 6 and 30 years were combined into a single, "mixed-type" functional connectivity maturation curve (figs. S5 and S6), with very similar properties to the pure 3-T rs-fcMRI maturation curve (Fig. 1). Six participants older than 30 years from data sets 2 and 3 were excluded from the fits for consistency across data sets. These findings demonstrate that fcMRI-based maturation analyses generalize across cohorts and different types of fcMRI data.

A crucial aspect of MVPA is displaying and analyzing the features that drive the multivariate predictor. Therefore, we extracted the weighting assigned to each feature (i.e., functional connection) by the predictor and displayed the 156 consensus features (*16*) from the SVR maturity prediction (data set 1) scaled by their weights (Fig. 2 and fig. S7). The resulting pattern of feature weights verified and expanded on findings from prior developmental rs-fcMRI studies (*7*, *8*, *27*). These previous studies, which were based on smaller sets of regions and sample numbers, had suggested that the brain's functional organization is dominated by more local

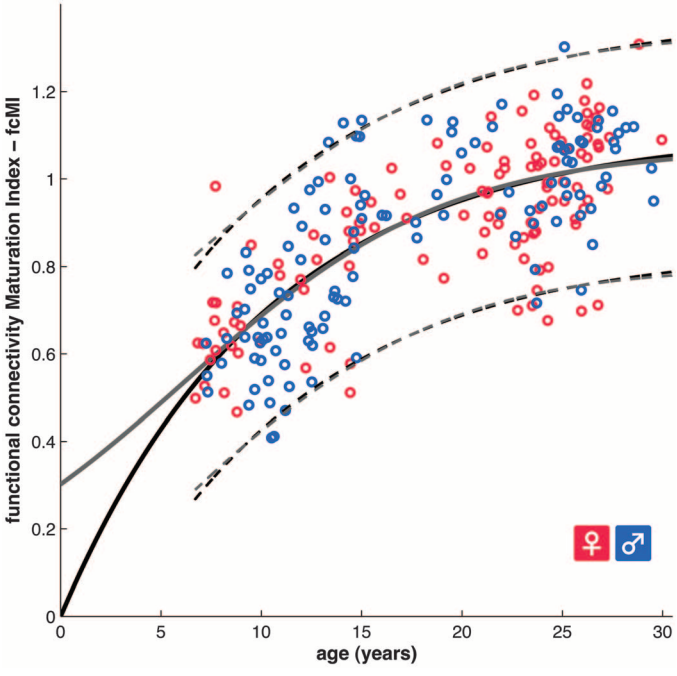

Fig. 1. Functional brain maturation curve. Individual functional brain maturity levels of 238 rs-fcMRI scans (115 females) between the ages of 7 to 30 years. Chronological age is shown on the x axis and the fcMI on the y axis (females pink, males blue). The fit for the Von Bertalanffy's equation [$a \bullet (1 - e^{-bx})$, $r^2 = 0.553$, permutation test, $P < 0.001$, AIC weight = 0.3] is shown with a solid black line. The fit for the Pearl-Reed equation [$a/(1 + b \bullet e^{-cx})$, $r^2 = 0.555$, AIC weight = 0.23] is shown with a solid gray line. The 95% prediction limits are shown with dashed lines.

interactions between brain regions in children and shifts to a more distributed architecture in young adults.

The fcMVPA brain maturity predictor has its basis in two types of functional connections, those whose strengths were positively correlated (strengthening) with chronological age and those that were negatively correlated (weakening) with chronological age (Fig. 2, figs. S7 and S8, and table S5). As previously noted (*7*, *8*, *27*), functional connections that grew in strength across development were significantly longer (mean = 80 mm) than functional connections that diminished in strength (37 mm) [$t(154) = 14.66$, $P < 1 \times 10^{-30}$] (figs. S7 and S8). In addition, we found that functional connections increasing in strength were significantly more likely to run along the anterior-posterior (AP) axis in the horizontal plane (mean angle = 37°) than the functional connections that became weaker (58°) [$t(154) = 4.84$, $P < 1 \times 10^{-5}$]. The quantitative nature of the MVPA approach also allowed us to extract the relative contributions of weakening and strengthening functional connections. These analyses revealed that weakening connections contributed more to predicting brain maturity (68%) than strengthening connections (32%), a finding better visualized by separately summing weights for both weakening and strengthening features (Fig. 3).

To extract the relative contributions of different ROIs to maturity prediction, we computed their node or ROI weights by summing the weights across all functional connections for each ROI (Fig. 2, fig. S9, and table S6).

Some of the regions in ventromedial prefrontal cortex and parietal cortex have previously been associated with the brain's default-mode network (*28*), whereas other anterior, dorsolateral, and medial prefrontal regions are known to be important for cognitive control (*4*, *6*, *29*). Hence, we assessed the network affiliations of each ROI more formally by performing modularity optimization on the average adult functional connectivity matrix (*8*). Doing so partitioned the 160 ROIs into six networks: cingulo-opercular, frontoparietal, default mode, sensorimotor, occipital, and cerebellar (Figs. 2 and 3 and fig. S9) (*8*, *30*).

Separately summing the feature weights for each network (Fig. 3) revealed that the cingulo-opercular control network had the greatest sum total of feature weights, meaning that it was the relatively best predictor, but all six identified networks made sizeable contributions toward predicting functional maturity. Separating functional connection weights according to whether the connections occur within or between networks (Fig. 3) revealed that the vast majority of predictor weights for within-network connections were assigned to strengthening connections (Fig. 3, left). In contrast, most of the weights for between-network connections were taken up by connections that weaken (Fig. 3, right). This pattern is consistent with the internal strengthening of the adult brains' six identified major functional networks, as well as the sharpening of the boundaries between them.

The region with the greatest relative prediction power about brain maturity was the right anterior prefrontal cortex [Montreal Neurological Institute (MNI): 27, 49, 26], thought to be important for cognitive control and higher-order

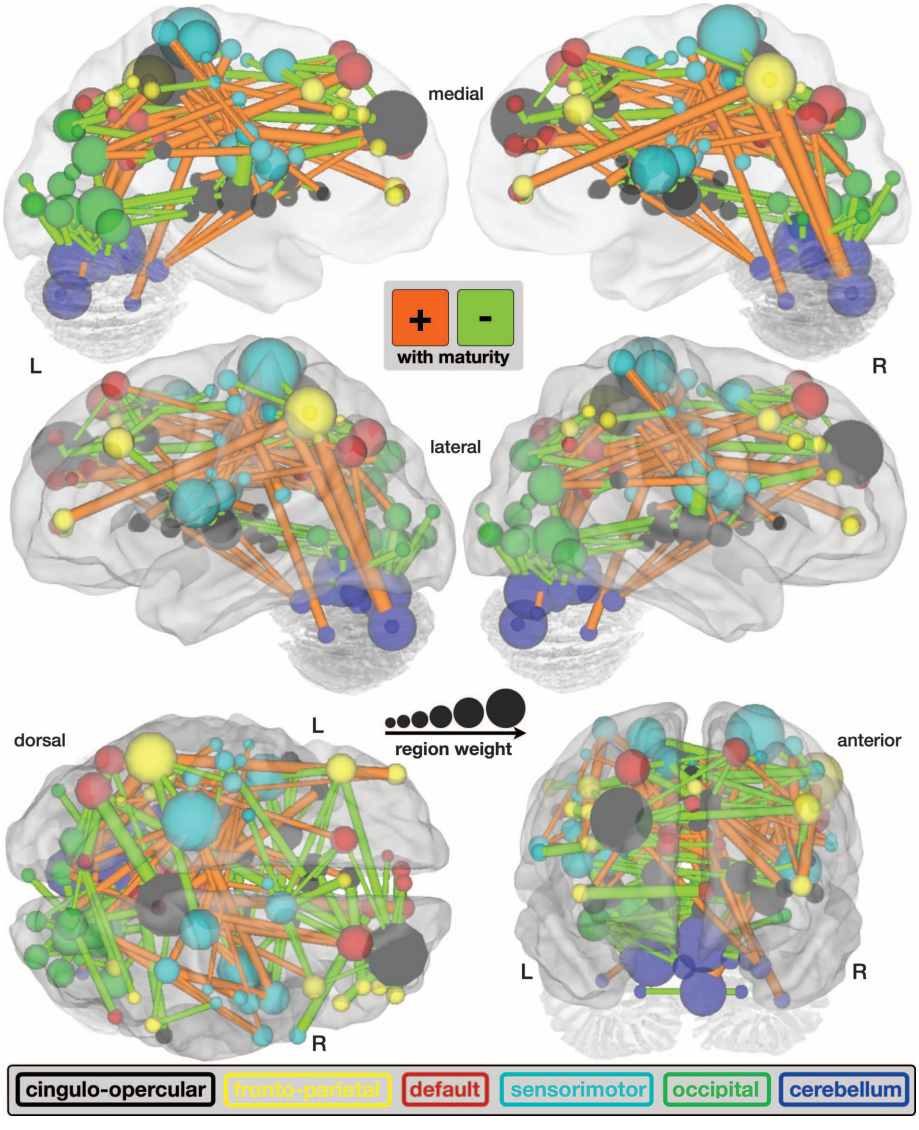

Fig. 2. fcMVPA connection and region weights. The functional connections driving the SVR brain maturity predictor are displayed on a surface rendering of the brain. The thicknesses of the 156 consensus functional connections scale with their weights. Connections positively correlated with age are shown in orange, whereas connections negatively correlated with age are shown in light green. Also displayed are the 160 ROIs scaled by their weights (1/2 sum of the weights of all the connections to and from that ROI). The ROIs are color-coded according to the adult rs-fcMRI networks (cingulo-opercular, black; frontoparietal, yellow; default, red; sensorimotor, cyan; occipital, green; and cerebellum, dark blue).

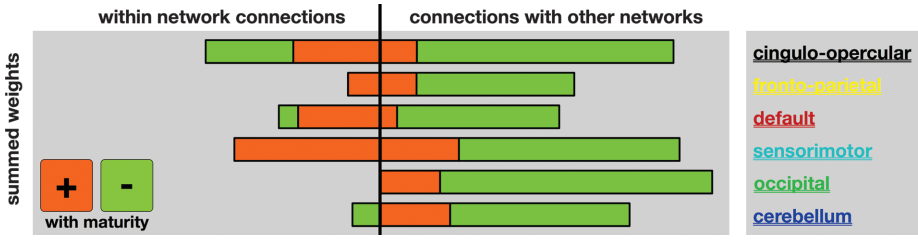

Fig. 3. SVR brain maturity weights by adult rs-fcMRI networks. The sums of all the functional connection weights within each network are shown to the left of the vertical black line. The sums of all the functional connection weights between networks are shown to the right.

reasoning (*4*, *6*, *9*, *29*). The precuneus, which has recently been found to be the most highly structurally (*31*) and functionally (*32*) connected brain region, contained the second most predictive ROI (MNI: 8, –40, 50). It stands to reason that regions such as those in the precuneus, situated at the center of the adult brain's connectome, could carry much information about how the network develops.

The results presented here strongly suggest that the fcMVPA approach derives its accuracy from important neurophysiologic changes. The functional connectivity maturation curve (Fig. 1 and fig. S6) has a biologically plausible asymptotic shape, first used to describe the growth of animals (Von Bertalanffy) and human populations in the setting of limited resources (Pearl-Reed) (*26*). Similarly shaped growth curves that plot measures such as height and head circumference against age are used routinely in pediatric medicine. The maturation curves suggest that mean population functional brain maturity asymptotes toward a maturity level or brain age of ~22 years (*33*). The shape of the functional maturation curve highlights the nonlinear nature of functional brain maturation (*34*, *35*).

The pattern of fcMVPA feature weights indicated that functional maturation is driven both by the segregation of nearby functional areas, through the weakening of short-range functional connections, and the integration of distant regions into functional networks, by strengthening of long-range functional connections (fig. S7) (*2*, *7*, *8*, *27*). It is interesting that fcMVPA revealed the relatively greater importance of functional segregation when compared to functional integration for the prediction of functional brain maturity. In addition, fcMVPA showed that functional integration is mainly carried by longer-range functional connections along the AP axis. Grouping brain regions into functional networks (*8*) showed that both integration within functional networks and segregation between them are widely distributed across the cortex and cerebellum.

Several important, large-scale structural MRI studies of brain maturation have already mapped out anatomical maturation curves for a variety of measures (*33*, *34*, *36*, *37*). The present study provides a functional counterpart to the prior anatomical studies. In addition, it combines the most relevant features into a single index instead of separately listing different measures. It should be informative to apply similar MVPA methods to the study of structural brain maturation, as well as combining MVPA of structural and functional data.

Important group-level rs-fcMRI studies have already shown differences in spontaneous activity in disorders such as autism, schizophrenia, depression, and attention-deficit hyperactivity disorder (*21*). Hence, imaging-based binary classification studies of clinical populations are starting to be pursued (*38*). The use of SVR in fcMVPA to make continuously valued predictions may become relevant in clinical scenarios where binary classification is insufficient (e.g., to predict years until Alzheimer's disease symptom onset).

The standard clinical workup for many developmental neuropsychiatric disorders already includes a structural MRI scan of the brain. The present observations suggest that the addition, at little extra cost, of a brief resting acquisition to the standard clinical study could one day provide useful information to aid in the screening, diagnosis, and prognosis of individuals with disordered brain function.

References and Notes

1. R. A. Poldrack, Y. O. Halchenko, S. J. Hanson, *Psychol. Sci.* **20**, 1364 (2009).
2. M. H. Johnson, *Nat. Rev. Neurosci.* **2**, 475 (2001).
3. T. Paus, M. Keshavan, J. N. Giedd, *Nat. Rev. Neurosci.* **9**, 947 (2008).
4. S. A. Bunge, N. M. Dudukovic, M. E. Thomason, C. J. Vaidya, J. D. E. Gabrieli, *Neuron* **33**, 301 (2002).
5. B. L. Schlaggar *et al.*, *Science* **296**, 1476 (2002).
6. E. A. Crone, C. Wendelken, S. Donohue, L. van Leijenhorst, S. A. Bunge, *Proc. Natl. Acad. Sci. U.S.A.* **103**, 9315 (2006).
7. D. A. Fair *et al.*, *Proc. Natl. Acad. Sci. U.S.A.* **104**, 13507 (2007).
8. D. A. Fair *et al.*, *PLOS Comput. Biol.* **5**, e1000381 (2009).
9. K. Velanova, M. E. Wheeler, B. Luna, *J. Neurosci.* **29**, 12558 (2009).
10. J. V. Haxby *et al.*, *Science* **293**, 2425 (2001).
11. S. M. Polyn, V. S. Natu, J. D. Cohen, K. A. Norman, *Science* **310**, 1963 (2005).
12. K. A. Norman, S. M. Polyn, G. J. Detre, J. V. Haxby, *Trends Cogn. Sci.* **10**, 424 (2006).
13. E. Formisano, F. De Martino, M. Bonte, R. Goebel, *Science* **322**, 970 (2008).
14. F. Pereira, T. M. Mitchell, M. Botvinick, *Neuroimage* **45**, S199 (2009).
15. A. Ben-Hur *et al.*, *PLOS Comput. Biol.* **4**, e1000173 (2008).
16. Materials and methods are available as supporting material on *Science* Online.
17. J. D. Johnson, S. G. R. McDuff, M. D. Rugg, K. A. Norman, *Neuron* **63**, 697 (2009).
18. T. M. Mitchell *et al.*, *Science* **320**, 1191 (2008).
19. C. S. Soon, M. Brass, H.-J. Heinze, J.-D. Haynes, *Nat. Neurosci.* **11**, 543 (2008).
20. A. Schurger, F. Pereira, A. Treisman, J. D. Cohen, *Science* **327**, 97 (2010); published online 12 November 2009 (10.1126/science.1180029).
21. D. Zhang, M. E. Raichle, *Nat. Rev. Neurol.* **6**, 15 (2010).
22. B. B. Biswal, F. Z. Yetkin, V. M. Haughton, J. S. Hyde, *Magn. Reson. Med.* **34**, 537 (1995).
23. B. B. Biswal *et al.*, *Proc. Natl. Acad. Sci. U.S.A.* **107**, 4734 (2010).
24. C. M. Lewis, A. Baldassarre, G. Committeri, G. L. Romani, M. Corbetta, *Proc. Natl. Acad. Sci. U.S.A.* **106**, 17558 (2009).
25. H. Akaike, in *Second International Symposium on Inference Theory,* B. N. Petrov, F. Csaki, Eds. (Akademiai Kiado, Budapest, 1973), pp. 267–281.
26. A. Tsoularis, J. Wallace, *Math. Biosci.* **179**, 21 (2002).
27. K. Supekar, M. Musen, V. Menon, K. J. Friston, *PLoS Biol.* **7**, e1000157 (2009).
28. M. E. Raichle *et al.*, *Proc. Natl. Acad. Sci. U.S.A.* **98**, 676 (2001).
29. N. U. F. Dosenbach *et al.*, *Neuron* **50**, 799 (2006).
30. N. U. F. Dosenbach *et al.*, *Proc. Natl. Acad. Sci. U.S.A.* **104**, 11073 (2007).
31. P. Hagmann *et al.*, *PLoS Biol.* **6**, e159 (2008).
32. D. Tomasi, N. D. Volkow, *Proc. Natl. Acad. Sci. U.S.A.* **107**, 9885 (2010).
33. F. I. M. Craik, E. Bialystok, *Trends Cogn. Sci.* **10**, 131 (2006).
34. P. Shaw *et al.*, *J. Neurosci.* **28**, 3586 (2008).
35. L. H. Somerville, B. J. Casey, *Curr. Opin. Neurobiol.* **20**, 236 (2010).
36. P. Shaw *et al.*, *Nature* **440**, 676 (2006).
37. G. Gong *et al.*, *J. Neurosci.* **29**, 15684 (2009).
38. H. Shen, L. Wang, Y. Liu, D. Hu, *Neuroimage* **49**, 3110 (2010).

39. This work was supported by NIH grants NS55582, NS053425, HD057076, and NS00169011 (B.L.S.); NS51281, NS32979, NS41255, and NS46424 (S.E.P.); DA027046 (C.N.L.-S.); EY16336 (J.R.P.); and MH62130 (D.M.B.) and by the John Merck Scholars Fund (B.L.S.), Burroughs-Wellcome Fund (B.L.S.), Dana Foundation (B.L.S.), Ogle Family Fund (B.L.S.), McDonnell Center (S.E.P. and B.L.S.), Simons Foundation (S.E.P.), American Hearing Research Foundation (J. E. C. Lieu), and Diabetes Research Center at Washington University (T. G. Hershey). We thank J. E. C. Lieu, C. E. Pizoli, and T. G. Hershey for providing data and F. M. Miezin, J. Harwell, A. Z. Snyder, and H. M. Lugar for help with data analysis.

Supporting Online Material

www.sciencemag.org/cgi/content/full/329/5997/1358/DC1
Materials and Methods
SOM Text
Figs. S1 to S9
Tables S1 to S6
References

23 June 2010; accepted 4 August 2010
10.1126/science.1194144